LAWRENCE
LIVERMORE
NATIONAL
LABORATORY

UCRL-JRNL-227877

MCSNA: Experimental Benchmarking of Pu Electronic Structure

J. G. Tobin

February 8, 2007

MCSNA: Experimental Benchmarking of Pu Electronic Structure

MCSNA:
Experimental Benchmarking of Pu Electronic Structure

J.G. Tobin
Lawrence Livermore National Laboratory
7000 East Ave, L-356, Livermore, CA, USA
Email: Tobin1@LLNL.Gov
Tele: 001-925-422-7247

I. Motivation and Overview

The objective of this work is to develop and/or apply advanced diagnostics to the understanding of aging of Pu. Advanced characterization techniques such as photoelectron and x-ray absorption spectroscopy will provide fundamental data on the electronic structure of Pu phases. These data are crucial for the validation of the electronic structure methods. The fundamental goal of this project is to narrow the parameter space for the theoretical modeling of Pu aging. The short-term goal is to perform experiments to validate electronic structure calculations of Pu. The long-term goal is to determine the effects of aging upon the electronic structure of Pu.

Many of the input parameters for aging models are not directly measurable. These parameters will need to be calculated or estimated. Thus a First Principles-Approach Theory is needed, but it is unclear what terms are important in the Hamiltonian. ($H\Psi = E\Psi$) Therefore, experimental data concerning the 5f electronic structure are needed, to determine which terms in the Hamiltonian are important. The data obtained in this task are crucial for reducing the uncertainty of Task LL-01-developed models and predictions. The data impact the validation of electronic structure methods, the calculation of defect properties, the evaluation of helium diffusion, and the validation of void nucleation models. The importance of these activities increases if difficulties develop with the accelerating aging alloy approach.

There are seven major papers, shown below, which encapsulate our results to date. This chapter will briefly discuss the contents of these papers and how they fit into the Enhanced Surveillance Campaign.

1. J.G. Tobin, B.W. Chung, R. K. Schulze, J. Terry, J. D. Farr, D. K. Shuh, K. Heinzelman, E. Rotenberg, G.D. Waddill, and G. Van der Laan, "Resonant Photoemission in f-electron Systems: Pu and Gd", **Phys. Rev. B 68**, 155109 (2003).
2. K.T. Moore, M.A. Wall, A.J. Schwartz, B.W. Chung, D.K. Shuh, R.K. Schulze, and J.G. Tobin, "The Failure of Russell-Saunders Coupling in the 5f States of Plutonium", **Phys. Rev. Lett. 90**, 196404 (2003).
3. G. van der Laan, K.T. Moore, J.G. Tobin, B.W. Chung, M.A. Wall, and A.J. Schwartz, "Applicability of the spin-orbit sum rule for the actinide 5f states," **Phys. Rev. Lett. 93**, 097401 (2004).
4. J.G. Tobin, K.T. Moore, B.W. Chung, M.A. Wall, A.J. Schwartz, G. van der Laan, and A.L. Kutepov, "Competition Between Delocalization and Spin-Orbit Splitting in the Actinide 5*f* States," **Phys. Rev. B 72**, 085109 (2005).
5. S.W. Yu, T. Komesu, B.W. Chung, G.D. Waddill, S.A. Morton, and J.G. Tobin, "f-electron correlations in nonmagnetic Ce studied by means of spin-resolved resonant photoemission," **Phys. Rev. B 73**, 075116 (2006).
6. B.W. Chung, A.J. Schwartz, B.B. Ebbinghaus, M.J. Fluss, J.J. Haslam, K.J.M. Blobaum, and J.G. Tobin, "Spectroscopic Signature of Aging in δ-Pu(Ga)," **J. Phys. Soc. Japan 75**, No. 5, 054710 (May 2006).
7. J.G. Tobin, S.W. Yu, T. Komesu, B.W. Chung, S.A. Morton, and G.D. Waddill, "Evidence of Dynamical Spin Shielding in Ce from Spin-resolved Photoelectron Spectroscopy," **Europhysics Lett**., **77**, 17004 (2007).

MCSNA:
Experimental Benchmarking of Pu Electronic Structure

II. Present Status
IIa. Present Status: Spectroscopic Signature of Aging in Pu

Resonant Photoemission, a variant of Photoelectron Spectroscopy, has been demonstrated to have sensitivity to aging of Pu samples, as shown in Figure 1. [Tobin et al, Phys. Rev. B. **68**, 155109 (2003).] The spectroscopic results are correlated with resistivity measurements and are shown to be the fingerprint of mesoscopic or nanoscale internal damage in the Pu physical structure. This means that a spectroscopic signature of internal damage due to aging in Pu has been established.

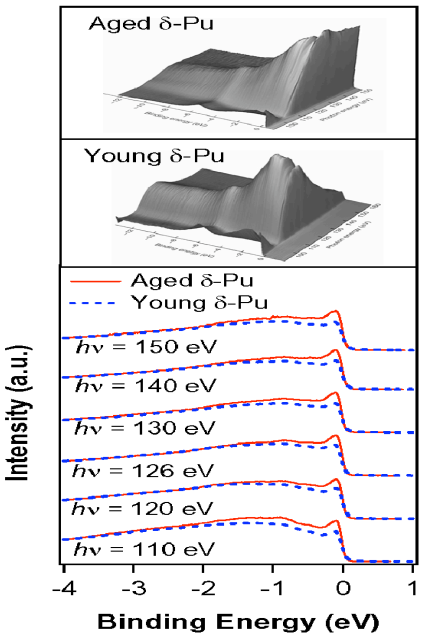

Figure 1
The RESPES results for a young, highly purified δ-Pu(Ga) sample are compared with the corresponding measurements of an aged δ-Pu(Ga), that is approximately 10 years old. In the topmost panels are the pseudo-three dimensional plots, with binding energy (0 to –12 eV) and photon energy (100 to 150 or 160 eV) as the in plane axes and the out of plane axis being intensity. Here, normalization is via flux measurements using a gold grid up-steam from the photoemission site. In the lower panel, comparison of the young (blue dashes) and aged (red lines) samples is made at specific photon energies, over the resonance regime photon energy range. In these lower panels, normalization is made at points above the Fermi Energy (0 eV) and at a binding energy of -4 eV.

Photoelectron spectroscopy is a “photon in, electron out” process. Often, it can be simplified down to a single electron phenomenon, where the energy of the photon is absorbed and transferred over entirely to a single electron, while all other “spectator” electrons essentially remain frozen. An advantage of this is its simplicity of interpretation. But in many systems, it is possible to induce a process with heightened sensitivity and significantly increased cross sections: resonant photoemission, shown schematically in Figure 2. Here, a second set of indirect channels open up, which contribute in concert with the original or direct channel of simple photoemission. In a naively simple theoretical picture, one can think of the intensity variations versus binding energy (relative to the Fermi energy) as being a measure of a self-convolution of the occupied valence electronic states. Shown in the Figure 1 are resonant photoemission results for two samples: single crystallite (large grain polycrystalline) delta and aged polycrystalline delta. The plots show intensity variations versus binding energy and photon (excitation) energy. Along the photon energy axis (90 eV to 160eV), the classical signature of resonant photoemssion can be seen: an anti-resonance or intensity minimum (near 100eV) followed by a maximum (near 125 eV). (These energies correlate with the Pu 5d core level threshold at 102eV: ResPes is a

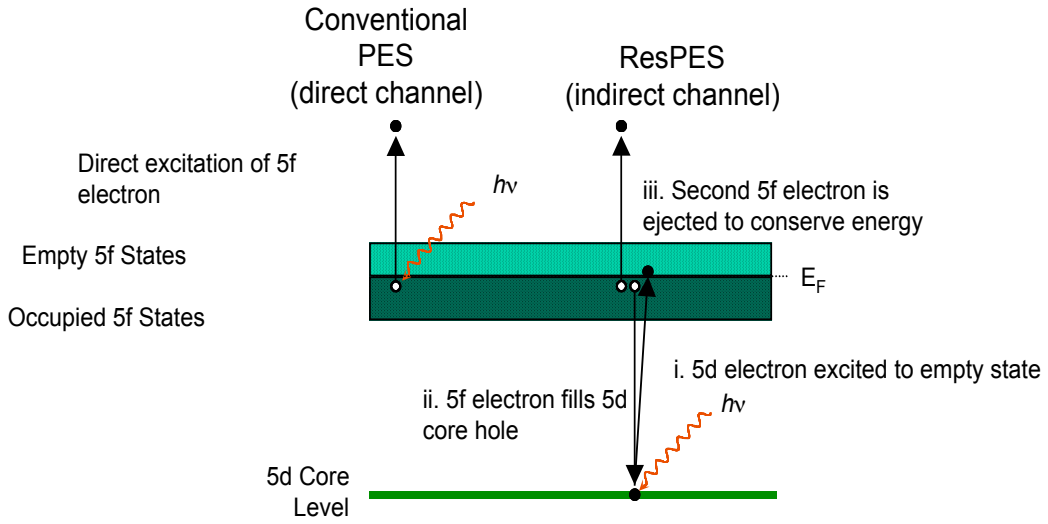

Figure 2:
Schematic of the resonant photoemission process. Photoemission is a "photon in-electron out" process. In conventional Photoelectron Spectroscopy, a single electron/ single channel is involved. In RESPES, additional indirect channels with multiple electrons can participate, increasing the cross section and sensitivity of the process.

multielectron process which in this case involves 5d as well as 5f electrons.) Along the binding energy axis, the "wall" is the threshold associated with the Fermi energy: no emission can occur above the Fermi Energy. While the overall envelopes of both data sets are approximately the same, as one might expect for two samples which are primarily Pu, the RESPES of aged sample is strikingly different than that of the young sample. To date, these are the strongest SPECTROSCOPIC effects observed in Pu due to aging

The cause of the difference in RESPES between aged and young samples is the nature of the screening and the associated possible decay channels. The highly ordered young samples have superior screening, giving rise to a quenching relative to the aged samples. Because of the mesoscopic disorder in the aged samples, the extra-atomic screening is compromised, allowing the resonant behavior to be amplified relative to the young samples. This illustrated in Figure 3A.

We can test this model of screening by correlating the RESPES results with resistivity measurements. It is clear that the underlying physics of the screening process and conductivity (the inverse of resistivity) would be the same. Diminished screening should thus correspond to diminished conductivity and greater resistance. At room temperature, many of the sources of the low temperature effects may have been eliminated by an effective "room temperature" annealing. Nevertheless, there has been strong evidence of aging effects in room temperature samples. For example, consider Figure 3B, where accelerated aging samples clearly show increases in length with time and hence dosage.

The effect of annealing a room temperature sample is demonstrated in Figure 3C. Two resistometry measurements are shown here: (1) a young δ-Pu(Ga) sample (blue dashes) and (2) an aged δ-Pu(Ga) sample (red line). The key effect is

observed at temperatures above 100°C: each sample is warmed from about 120°C to about 300°C (and then cooled to about 40°C). The aged sample exhibits a sharp drop in resistance, while the resistance of the young sample is constant. The drop in the resistance of the aged sample is a strong indication of the annealing out of the residual internal damage in the aged sample. The aged sample was 18 years old.

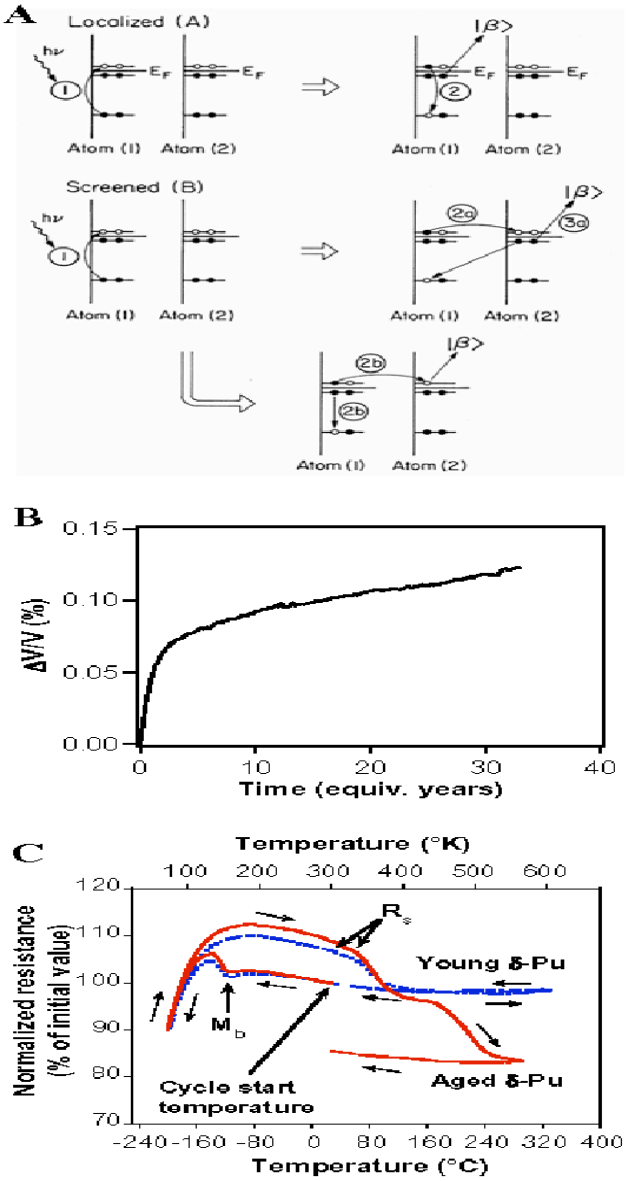

Figure 3
*A) Intra- and extra- atomic channels of decay in the resonant photoemission process. Taken from Dowben [Surface Science Reports **40**, 151 (2000).].*
*B) Here is shown the sample length expansion of δ-Pu(Ga) with aging at room temperature [Symp. Proc. Matl. Res. Soc. **802**, 39 (2004).]. In this case, accelerated aging was achieved by doping a Pu239 sample with 7.5 weight % of Pu238. The time equivalent in regular years is shown as the x-axis.*
C) Normalized Resistance vs T(°C): The effect of annealing upon the normalized resistance of room temperature δ-Pu(Ga) is shown here.

Taken from: B.W. Chung, A.J. Schwartz, B.B. Ebbinghaus, M.J. Fluss, J.J. Haslam, K.J.M. Blobaum, and J.G. Tobin, "Spectroscopic Signature of Aging in δ-Pu(Ga), J. Japan. Phys. 2006.

To summarize: Increased screening quenches the RESPES, radiological damage restricts the screening in the aged sample and thus the aged sample has more RESPES. We now understand the spectroscopic signature of aging in Pu.

MCSNA:
Experimental Benchmarking of Pu Electronic Structure

IIb. Present Status: Fundamental Studies of Pu Electronic Structure

We are unraveling the enigma of Pu electronic structure. Sixty years after its discovery, the mystery of the electronic structure of Pu is finally being resolved. In a series of experiments and linked theoretical modeling, the range of possible solutions for Pu electronic structure has been dramatically reduced.

Our approach is to experimentally determine which potential terms are the largest.

$$H\Psi = -(\nabla^2/2m)\Psi + V\Psi, \qquad \text{where } V= V_1 + V_2 + V_3 + V_4 + \ldots$$

Synchrotron-radiation-based X-ray absorption, electron energy-loss spectroscopy in a transmission electron microscope, multi-electronic atomic spectral simulations and first principles calculations (Generalized Gradient Approximation in the Local Density Approximation, GGA/LDA) have been used to investigate the electronic structure of Pu. From these studies, we have gleaned the following key insights.

1. Russell-Saunders Coupling fails for Pu and the number of 5f electrons in Pu is approximately 5.
2. Pu is a jj-skewed Intermediate Coupling case, with a large 5f spin-orbit coupling. Spin orbit splitting dominates delocalization effects: $V_{SO} > V_{Delocalization}$, to the point that the Pu 5f states can be viewed as predominantly localized.

Each of these insights will be discussed below. The key enabling measurements were x-ray absorption spectroscopy (XAS, Figure 4) and high energy electron energy loss spectroscopy (EELS). Under normal conditions, the utility of EELS is limited by its coulombic matrix elements that govern its transitions and complicate its spectrum. However, under the limiting conditions of high-energy excitation and low energy transitions, EELS becomes dominated by the electric dipole matrix elements and converges to a limit very similar to the intrinsically simpler and more fundamental XAS. In these studies, EELS results have been experimentally verified by comparison with XAS spectra of Pu.

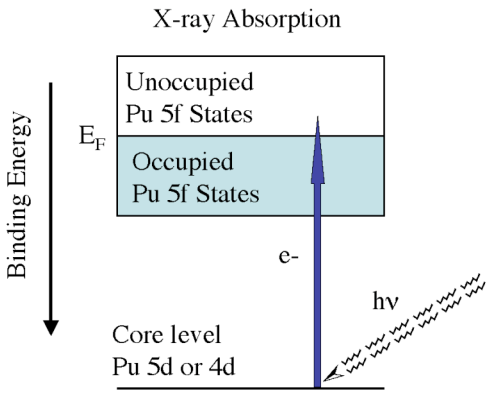

Figure 4
Schematic illustration of the x-ray absorption process. E_F is the Fermi Level, the energy level between the occupied and unoccupied states. The photon ($h\nu$) is absorbed, moving the core level electron (e-) up into the unoccupied states.

MCSNA:
Experimental Benchmarking of Pu Electronic Structure

IIb1. Russell-Saunders Coupling fails for Pu and the number of 5f electrons is approximately 5. (Please see PRL 90, 196404 (2003) for references and details.)

The nature of Pu 5f electronic structure is still under debate. Many of the complications are derived from the necessity of explaining the phase-specific behavior of Pu and Pu alloys, particularly the low symmetry (monoclinic) α phase and the high symmetry (fcc) δ phase. Experimentally, there are severe hindrances, such as the general lack of single crystals and the radioactive and chemical hazards of the materials. Theoretically, no single model has gained universal acceptance, because of the limitations of each approach. Recent advances include the application of Dynamical Mean Field Theory (DMFT) to δ-Pu, Generalized Gradient Approximation with a Hubbard U (GGA-U) to δ-Pu, Density Functional Theory with Gradient Density Corrections and spin-orbit polarization to α-Pu and δ-Pu. Yet many of the same questions remain from earlier formulations. Several of these key questions revolve around the interaction of the spin and orbital angular momenta. In fact, until now, it was even unclear which momentum-coupling scheme should be used with the Pu 5f states.

To digress, there are two limiting cases for the coupling of angular momenta in multi-electronic systems: Russell Saunders or LS coupling and jj coupling. It has been shown that while the two schemes produce similar trends in derived quantities, there is an important "shift" between the results of the two schemes, thus generating very different results on an element by element basis. Historically, it has been demonstrated that the Russell-Saunders approach has been generally very successful with the Rare Earths and the earlier modeling of of actinides was based upon a non-relativistic approach, i.e. neglecting spin-orbit splitting. More recent calculations have either explicitly included the spin-orbit splitting or generated results that are consistent with a jj scheme. jj coupling should become appropriate as the atomic number increases. Nevertheless, until now there remained significant uncertainty about which coupling scheme was appropriate.

Using Synchrotron- Radiation- based X-ray Absorption Spectroscopy (XAS), High Energy – Electron Energy Loss Spectroscopy (HE-EELS), and Transmission Electron Microscopy (TEM), we have shown that Russell- Saunders (LS) coupling fails for the 5f states of Pu. A jj coupling scheme is necessary to explain our experimental observations. This result has important consequences for the future direction of efforts to resolve the open questions of Pu 5f electronic structure. Because microscopic focusing is used in the HE-EELS experiments, the measurements are completely phase specific.

The absence of pre-edge structure in the X-ray Abs of Pu indicates the failure of RS coupling.

RS versus JJ Coupling

For two particles (1,2) and 4 angular momenta (l_1,l_2,s_1,s_2)

RSJJ

$L = l_1 + l_2$	$j_1 = l_1 + s_1$
$S = s_1 + s_2$	$j_2 = l_2 + s_2$
$J = L + S$	$J = j_1 + j_2$

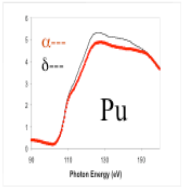

↑ No Pre-edge Peaks

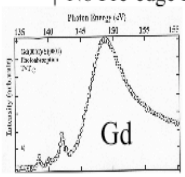

↑ ↑ Pre-edge Peaks

Figure 5
The spectrum of the 5d to 5f XAS transition of Pu is shown here, along with the spectrum of the 4d to 4f XAS transition of Gd. The absence of pre-edge structure indicates that Pu cannot be an RS coupling case and that the number of Pu 5f electrons must be approximately 5.

Let us consider this a little more carefully. The analogous transition in the Rare Earths is $4d^{10}4f^{N} \rightarrow 4d^{9}4f^{N+1}$. Obviously, when n=14, no transitions will occur. For almost all of the rare earth element series, the same spectral shape is observed: sharp, pre-peak structure at lower photon energies followed by a broad continuum peak at higher photon energies, as shown for Gd in Figure 5. This behavior has been explained previously by Dehmer et al., Starace and Sugar. The coulombic and exchange interactions between the partially occupied 4d and 4f final state levels drive the splitting of these angular-momentum-coupled states, generating energy splittings on the scale of 20 eV. The pre-peak structure can persist as individual peaks but at higher photon energies, where the outgoing electron can actually escape, coupling to the continuum generates a large, broad peak, which is sometimes referred to as the giant resonance. Sugar predicts that for $4f^{13}$, only a single line should be observed. Because of the interaction of the 4f and 5d6s manifolds, the f states do not necessarily fill monotonically. The situation can be further complicated by the presence of separate and different valencies on the surface and in the bulk. The best observation of the end of series behavior is in Yb and YbO by Johnsson et al. Yb ($4f^{14}$) shows no edge or line but YbO ($4f^{13}$) exhibits a single, fairly broad peak. Thus, the characteristics of filling the rare earth 4f shell is (1) the loss of pre-peak structure at an initial state of $4f^{13}$ and (2) the absence of any feature at an initial state of $4f^{14}$. If one applies this logic to Figs. 5, the conclusion is inescapable: In Pu the $5f^{5/2}$ level is being filled by $5d^{10}(5f^{5/2})^{5} \rightarrow 5d^{9}(5f^{5/2})^{6}$. In the 4f levels of the Lanthanides, where Russell-Saunders coupling is occurring, the only filling effects can be seen at the end of the series. (Half filling is possible, but doesn't seem to be important: it may be obfuscated by the effects of multiple 4f valencies and interactions with the 5d6s manifold.) In the actinides, the filling can be seen to occur mid-series, when the ($5f^{5/2}$) occupation goes from 5 to 6 in the process of XAS or EELS. It is possible to partially fill the ($5f^{7/2}$) level: Pu $5d^{10}(5f^{5/2})^{5}(5f^{7/2})^{0} \rightarrow 5d^{9}(5f^{5/2})^{5}(5f^{7/2})^{1}$. However, this should occur at higher photon energies and fall within the large, broad feature associated with transitions into the continuum. Thus, it is expected that the single, fairly broad peak from the ($5f^{5/2}$) level and all of the ($5f^{7/2}$) features should become part of the giant resonance peak.

To summarize, the XAS data for the 5d to 5f transition in Pu demonstrates the failure of RS coupling for Pu and the necessity of n =5 for the Pu 5f states. These conclusion were reached without the need for spectral simulations of Pu!

IIb2. Pu is a jj-skewed Intermediate Coupling case, with a large 5f spin-orbit coupling. Spin orbit splitting dominates delocalization effects: $V_{SO} > V_{Delocalization}$, to the point that the Pu 5f states can be viewed as predominantly localized.

(Please see PRL 93, 097401 (2004) and PRB 72, 085109 (2005) for references and details.)

In section IIb1 above, the 5d to 5f transition, with an energy of about 100 eV, was used to probe the electronic structure of Pu. An alternative route is to use the 4d to 5f transition, again with electric dipole matrix elements of XAS, to interrogate the electronic structure of Pu. The 4d to 5f transitions occur at an energy of about 800 eV. Because deeper core levels are being used, there is a larger core level spin-orbit splitting, on the scale of 50 eV, separating the intensities into two well defined peaks, the $4d^{5/2}$ and the $4d^{3/2}$. One manifestation of dipole selection rules is that 3/2 to 7/2 transitions are forbidden. Thus, as the $5f^{5/2}$ levels fill up, the intensity of the $4d^{3/2}$ peak will drop dramatically. In fact, we have observed this in the Pu XAS and EELS spectra, shown in Figure 6.

MCSNA:
Experimental Benchmarking of Pu Electronic Structure

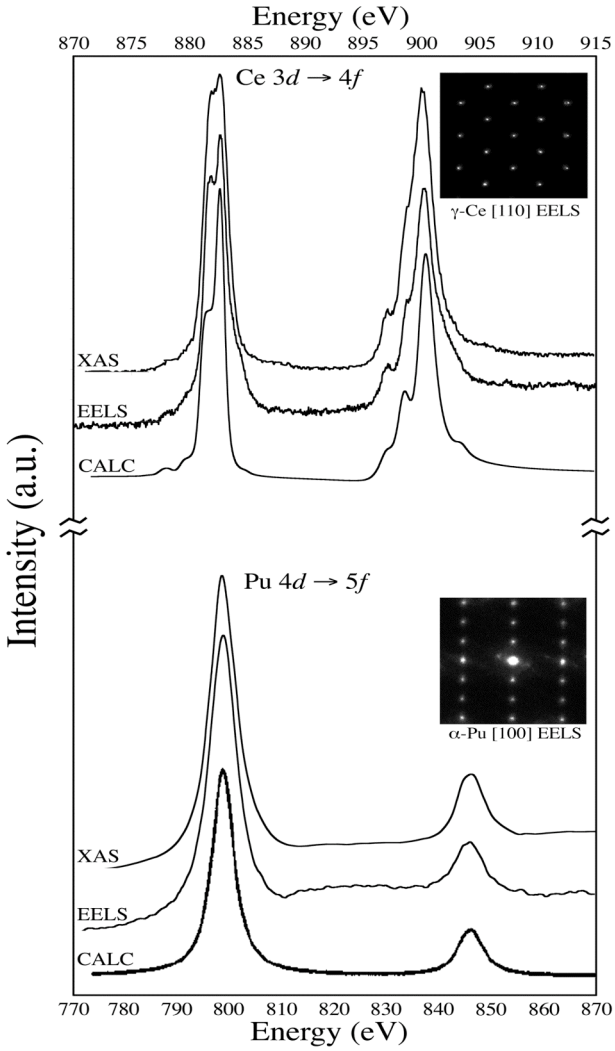

Figure 6.
White line spectra α-Pu ($N_{4,5}$,4d→5f) and Ce ($M_{4,5}$,3d→4f) acquired by XAS, EELS in a TEM, and spectral simulation are shown here. A single-crystal diffraction pattern from each metal is presented, confirming the phase being examined by EELS. For Ce, the $3d^{5/2}$ peak is near 884 eV and the $3d^{3/2}$ peak is near 902 eV. For Pu, the $4d^{5/2}$ peak is near 798 eV and the $4d^{3/2}$ peak is near 845 eV. Note the significantly different energy scales for the Ce and Pu

For comparison, the spectra of the corresponding 3d to 4f transitions of Ce are also shown in Figure 6. In the case of Ce, the 4f's are almost completely empty, so the attenuation of the 3/2 peak is minimal.

In order to quantify the analysis of this transition, the intensities of the peaks were determined and then converted into Branching Ratios (B), where $B = I_{5/2} (I_{5/2} + I_{3/2})$. Subsequently, these branching ratios were converted into spin-orbit moments, <w110>. By comparing the experimental results with atomic calculations for the RS Limit, jj Limit and Intermediate Coupling Case, we can use the spin-orbit interaction as a measure of the degree of localization of valence electrons in a material. In order to get the systematics within the actinide series, the spin-orbit interactions in the light actinide metals, α-Th, α-U and α-Pu, hav been determined using the branching ratio of the white line peaks of the $N_{4,5}$ edges, which correspond to 4d -> 5f transitions. Examination of the branching ratios and spin-orbit interaction shows that the apparent spin-orbit splitting is partially quenched in α-U, but is strongly dominant α-Pu. These results are fully quantified using the sum rule.

MCSNA:
Experimental Benchmarking of Pu Electronic Structure

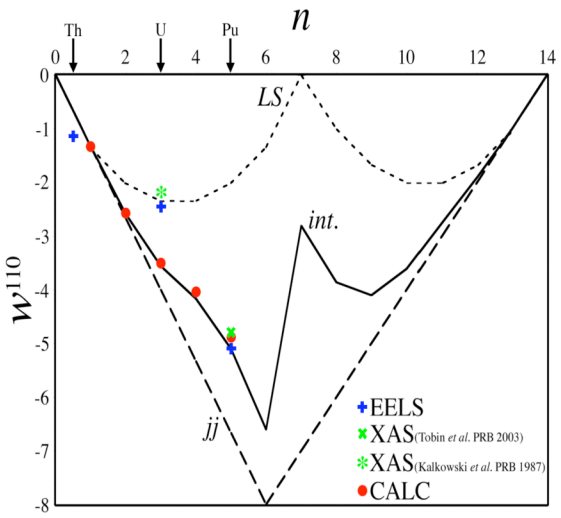

Figure 7.
A plot of the expectation value of the spin-orbit operator <w^{110}> as a function of the number of 5f electrons (n). The three different electron coupling schemes, within an atomic (localized) model, are plotted; LS (short dash), jj (long dash), and intermediate coupling (solid). Notice how U falls directly on the LS curve, while Pu falls directly on the Intermediate Coupling curve. This demonstrates that that the Pu 5f electronic structure is a jj-skewed intermediate case, with a predominance of the spin-orbit over delocalization. However, in U the delocalization is stronger and mixes the 5f states, inducing an accidental agreement with the LS model.

This picture of the actinide 5f electronic structure is confirmed by comparison with the results of electronic structure calculations for α-Th, α-U and α-Pu, which in turn are supported by a previous Bremstrahlung Isochromat Spectroscopy (BIS) experiment (Figure 8).

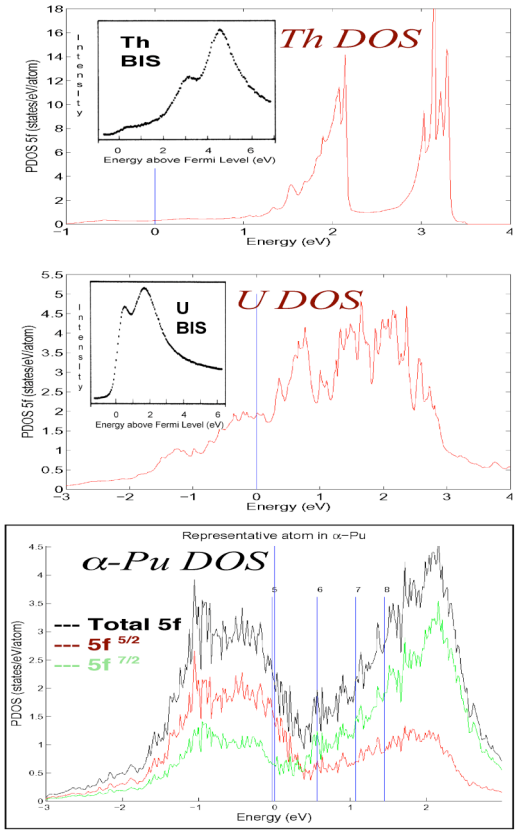

Figure 8.
*DOS of α-Th, α-U and α-Pu, as described in the text. The Th and U BIS data, shown as inserts, is from Baer and Lang [Phys. Rev. B **21**, 2060 (1980)]. The blue vertical lines with numerical annotations in the α-Pu calculation correspond to various occupations (n) of the Pu 5f states. For Pu, n ≈ 5.*

The calculations of Th, U and Pu were performed by A.L. Kutepov of Russian Federation Nuclear Center, VNIITF, Snezhinsk, Russia, under an inter-lab agreement between LLNL and VNIITF. ALK is a co-author on the 2005 PRB.

From these calculations, it is determined that the 5f spin-orbit splitting is approximately 2eV in Pu. This large value is consistent with a jj- skewed intermediate case and the dominance of the spin-orbit effect over the delocalization in the Pu 5f states.

The spin-orbit split, two-lobe structure is clearly visible in the case of α-Th and this is consistent with Bremstrahlung Isochromat Spectroscopy (BIS) result of Baer and Lang [Phys. Rev. B **21**, 2060 (1980)], shown as an inset. Because of the high energy (1487 eV) of the transition used in BIS, the BIS spectrum can provide a fairly accurate if somewhat broadened picture of the unoccupied density of states above the Fermi Level. (Thus in comparing BIS to the DOS calculations here, one should only look at the calculated DOS above the Fermi Level. In BIS, the spectral transitions are forbidden to states below the Fermi Level, leading to a sharp drop-off or step at the Fermi Level (E = 0 eV) in the BIS data.) In the middle panel, the corresponding results are shown for α-U. Again, there is a strong agreement between the calculated DOS and the BIS of U, if the "1 eV" broadening of the BIS measurements is taken into account, with peaks at 1/2 eV and 2eV and a minimum near 1 eV, relative to the Fermi Level at 0 eV. Here again, the impact of increased relative delocalization in U can be observed: instead of two strongly lobed features as in Th and Pu, the DOS of U is "smeared out," above and below the Fermi Level.

Finally, in the lowermost panel of Figure 3, the DOS of a representative atom from α-Pu is shown, with a breakdown into states composed of $5f^{5/2}$ and $5f^{7/2}$ origin. Clearly, the lower lobe is predominantly of $5f^{5/2}$ character and the upper lobe is predominantly of $5f^{7/2}$ character, but significant mixing is occurring, consistent with the Intermediate Coupling model used in the spectral analysis above. **Thus it is obvious: even in α-Pu, the delocalization perturbation is a secondary effect relative to the spin-orbit splitting of the 5f states.**

The remaining issues for Pu electronic structure are mainly those of electron correlation effects. Based upon the success of magnetic methods in explaining the physical properties of the different phases of Pu [P. Soderlind and B. Sadigh, Phys. Rev. Lett. (2004); P. Soderlind, A. Landa, and B. Sadigh, Phys Rev. B (2002) and B. Sadigh, P. Soderlind and W. Wolfer, Phys. Rev. B (2003).], it is possible to hypothesize that for δ-Pu there are strong indications that V_{MAG} perturbs V_{SO} and $V_{MAG} > V_{Delocalization}$. In Pu, we expect to observe large but counter aligned spin and orbital polarizations or magnetic moments within the 5f manifold. The counter alignment should lead to substantial cancellation. However, there would need to be an additional shielding or cancellation going on in δ-Pu, such as Kondo Shielding, Spin Fluctuation, Non-Collinearity, or Averaging. Alternatively, there is the possibility that there are no magnetic effects and that the electron correlation is a type of Kondo shielding best described by Dynamical Mean Field Theory. (Kotliar and Vollhardt, Physics Today, March 2004, Saravsov, Kotliar and Abrahams, Nature (2001).] We can resolve these last two issues with the Fano Effect measurements, as will be described below.

Our approach is founded upon a model in which spin and spin-orbit splittings are included in the picture of the 5f states and upon the observation of chiral/spin-dependent effects in non-magnetic systems. By extending a quantitative model developed for the interpretation of core level spectroscopy in magnetic systems, it is possible to predict the contributions of the individual component states within the 5f manifold. This has lead to a remarkable agreement between the results of the model and the previously collected spectra of δ-Pu.

MCSNA:
Experimental Benchmarking of Pu Electronic Structure

IIIa. Fano Effect Measurements

Let us digress for a moment and reconsider the Pu Density of States (DOS). In our recent PRB, Kutepov calculated both a non-magnetic (NM) and Anti-Ferromagnetic (AF) DOS. Both agree qualitatively with our simple picture derived from spectroscopic results. The NM and AF limits are related, being on opposite ends of the plot below in Figure 10. (For NM, Hs/ζ = 0, and for AF, the extreme limit would be Hs/ζ > 10. *Here Hs = Spin Field (Exchange) and ζ = Spin-Orbit Parameter*) What about an intermediate solution?

Simple Picture derived from the spectroscopic analysis

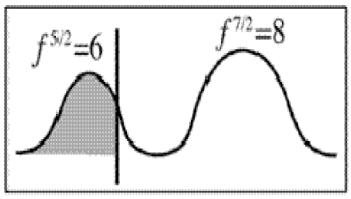

Result of non-magnetic calculation, including spin-orbit in the Pu 5f's

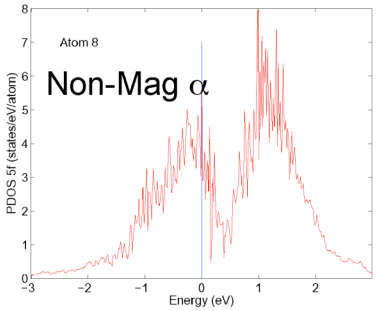

Result of anti-ferromagnetic calculation, including spin-orbit in the Pu 5f's

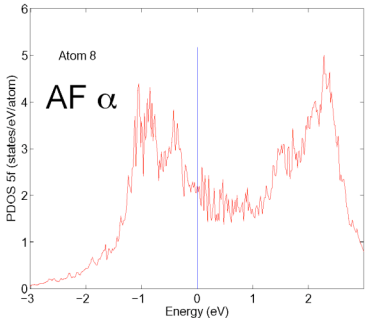

Figure 9
The Pu DOS.

One way to extract the possible size of the magnetic perturbation would be to analyze the X-ray Absorption Branching Ratio of Pu, assuming a jj limit with a magnetic splitting. We have done that and the result is shown below in Figure 10.

Here we have analyzed the Pu 4d to 5f XAS data, shown in Figure 6, with a simple one electron picture with 5 electrons in the 5f level (n = 5), magnetically polarized 5f states, and linear photon polarization, including the correct state to state transition cross sections within the electric dipole approximation. The branching ratio analysis gives the result that Hs/ζ = 2.5. (See Figure 10.) From Kutepov's calculations we know that $\Delta E_{SO} \approx 2$ eV and using Hs/ζ = 2.5, we obtain $\Delta E_{MAG} \approx 0.2$ eV.

MCSNA:
Experimental Benchmarking of Pu Electronic Structure

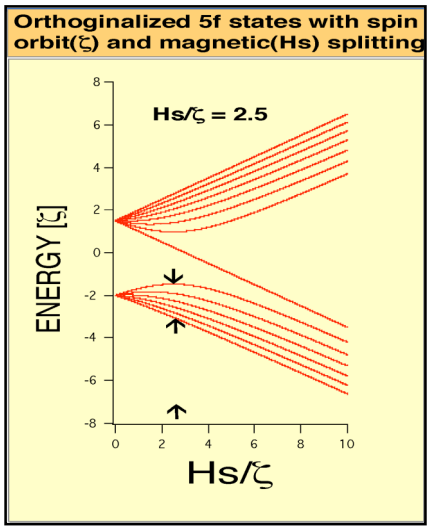

Figure 10
Determining the location of the intermediate solution, using the experimental XAS B results.

Our new model can explain the "regular" photoemission results for δ-Pu. Using the value of Hs/ζ = 2.5 and including the correct state to state transition cross sections within the electric dipole approximation for Photoelectron Spectroscopy (PES), the magnetic perturbation model (V_{SO} + V_{MAG}) gives fairly good agreement with our data, bulk δ and bulk α with a δ reconstruction: at worst, the model result is semi-quantitatively correct. Interestingly, the model is closer to the results of Butterfield et, where the small remaining oxygen-driven contributions have been reduced even further. Please note that our model has no delocalization nor hybridization in it. In the 5f states, delocalization and hybridization are essentially the same. Thus the result of this analysis suggests that hybridization and delocalization play a role in the δ-Pu 5f states but it is a TERTIARY role…..V_{SO} > V_{MAG} > $V_{Delocalization}$.

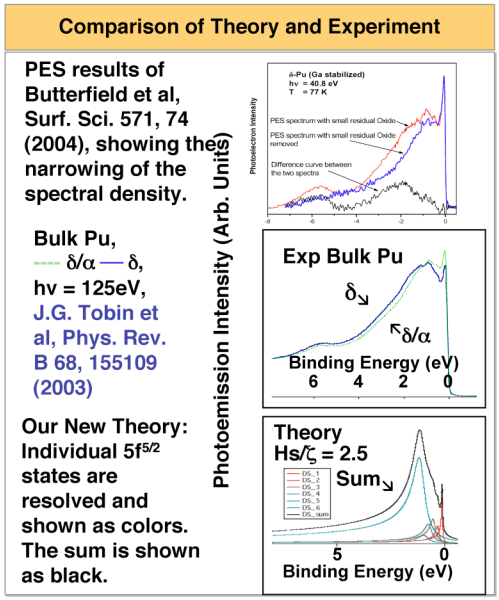

Figure 11
PES Experiment and Theory. The theory here is NOT Density of States (DOS) but rather spectral simulations with correct state-to-state matrix elements.

MCSNA:
Experimental Benchmarking of Pu Electronic Structure

The acid test of our new model of Pu electronic structure will be the spin dependence. Using the Fano Effect (Double Polarization Photoelectron Dichroism), we should see a strong spin dependence in Non-Magnetic Pu, as shown in Figure 12. The Fano Effect is the emission of spin polarized electrons by NONMAGNETIC materials, when excited by circularly polarized photons, as predicted by U. Fano [Phys. Rev. 178, 131 (1969); 184, 250 (1969)] and measured by U. Heinzmann, J. Kessler, and J. Lorenz [Phys. Rev. Lett. 25, 1325 (1970)]. Fano Dichroism PES is the ideal technique with which to probe for such a dynamically shielded moment, with (1) a probe time on the scale of 10^{-18} seconds and (2) the capability to see spin effects in nonmagnetic materials!!

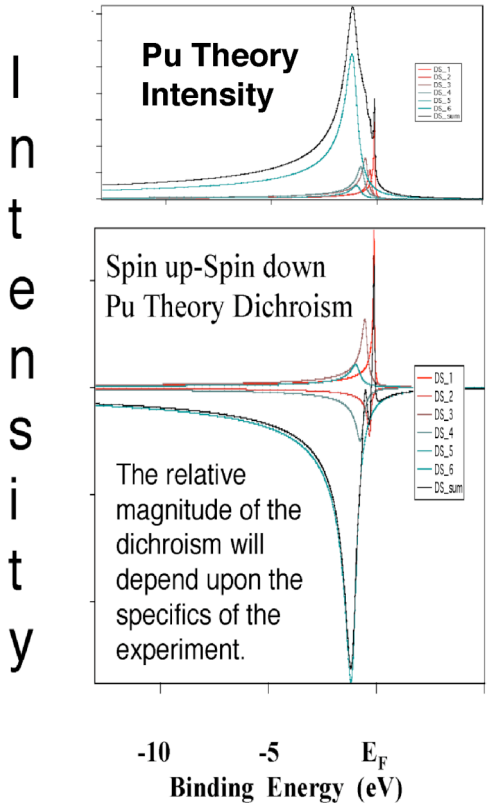

Figure 12
Pu Theory PES and Fano Dichroic Intensities.

At this point, it is useful to digress again and consider the "Fano Effect" and its special characteristics in more detail. We believe that Fano effect measurements (aka Double Polarization Photoelectron Spectroscopy, DPPS) are the key to unraveling the electron correlation in Pu. In Fano Effect measurements, one uses a chiral excitation and true spin detection of the electrons in NONMAGNETIC materials to gain detailed information about the valence band electronic structure of these materials. In ferro-magnetic systems, it is necessary to have only single polarization because of the presence of the macroscopic magnetization vector. In the case of ferro-magnetic systems with a double polarization experiment, the major improvement is in increasing the magnitude of the observed effects, at the cost of raw signal rate. In non-magnetic systems with single polarization, no effect is observed. In order to see the underlying spin characteristics in non-magnetic systems, one must resort to double polarization experiments.

MCSNA:
Experimental Benchmarking of Pu Electronic Structure

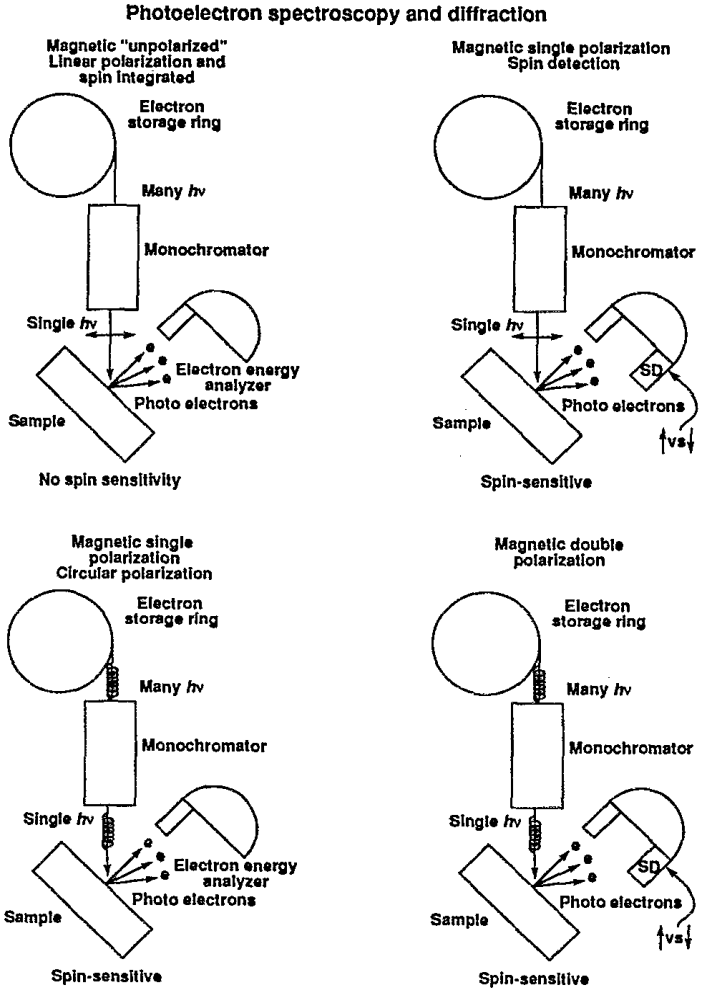

Figure 13
Top,left- unpolarized; Bottom, left-single polarization due to circularly polarized x-rays;
Top, right- single polarization due to spin detection;
Bottom, right- double polarization photoelectron dichroism. It should be noted that although we show the "unpolarized" case with linear polarization, it is possible to use linearly polarized or unpolarized x-radiation as part of a chiral arrangement, to achieve X-ray Magnetic Linear Dichroism in PES. Here the chiral arrangement of vectors essentially mimics the intrinsic chirality of the circularly polarized x-rays

.

We are pursuing this investigation in a two-pronged fashion: (a) calibration studies of Ce, the 4f analogue of Pu, at synchrotron radiation sources; and (b) in house studies of Pu.

Although we have not yet been able to carry out the Pu Double Polarization experiment, we have been able to test the feasibility of this approach using Ce, the Rare Earth element analog of Pu. Shown in the section below are our preliminary results for Double Polarization Photoelectron Spectroscopy of polycrystalline γ–Ce, using both circularly polarized x-rays and spin resolving detection.

MCSNA:
Experimental Benchmarking of Pu Electronic Structure

IIIb. Spin-Resolved Electronic Structure Studies of Non-Magnetic Systems: Possible Observation of the Fano Effect in Polycrystal Ce

The valence electronic structure and electron spectra of Cerium remain a subject of uncertainty and controversy. Perhaps the best and most direct method of ascertaining the valence electronic structure is the application of electron spectroscopies [1-17], e.g. photoelectron spectroscopy for the occupied states [1-10, 12-14] and x-ray absorption [2] and Bremstrahlung Isochromat Spectroscopy (inverse photoelectron spectroscopy) [3,11,13] for the unoccupied states. Much of the controversy revolves around the interpretation of the Ce photoemission structure in terms of a modified Anderson Impurity Model [15,16]. Here, in this correlated and multi-electronic picture, semi-isolated 4f states (at a nominal binding energy of 1 eV) are in contact with the bath of spd valence electrons, generating spectral features at the Fermi Level and at a binding energy corresponding to the depth of the bath electron well, about 2 eV below the Fermi Level in the case of Ce. This controversy has spilled over into issues such as the volume collapse associated with the alpha to gamma phase transition [17-19] and the electronic structure of Ce compounds [20-23]. (A more generalized schematic illustrating the competition between the bandwidth (W) and correlation strength (U) is shown in Figure 14.) Considering the remaining uncertainty associated with the spectral features and valence electronic structure of Ce, it seemed plausible that the situation would benefit from the application of a spectroscopy with increased resolution and probing power. To this end, we have applied circularly polarized soft x-rays and true spin detection, in a modified form of the photoelectron spectroscopy experiment, to the enigmatic Ce system. The result of this is that we have observed the first evidence of the Fano Effect in the valence electronic features of non-magnetic Cerium ultra-thin films.

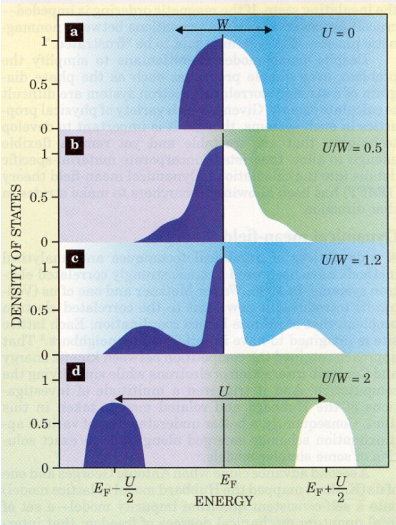

Figure 14
Illustration of the origin of the quasiparticle (at the Fermi Level, E_F) and the Hubbard Bands (at $\pm U/2$, relative to the Fermi Level). W is the band width and U is the correlation strength. Case c, third from the top, is the case closest to Ce. Taken from Ref 24.

The Fano Effect is the observation of spin specific photoelectron emission from the valence bands of a non-magnetic material due to excitation with circularly polarized light. First predicted in 1969 by Fano [25], the effect was experimentally confirmed by measuring the polarization of alkali vapor beams using detection of ions [26-28] and photoelectron emission [29] shortly thereafter. Subsequently, the effect was observed in the spin resolved photoemission of non-alkali systems, including the heavy atoms such as Th [30], Hg [31], and Xe/Pd (111) [32]. A variation of the Fano effect, in the core level photoemission of non-magnetic materials, has also been measured using both circular dichroism [33] and linear dichroism [34,35]. Our data for Au is shown in Fig 15.

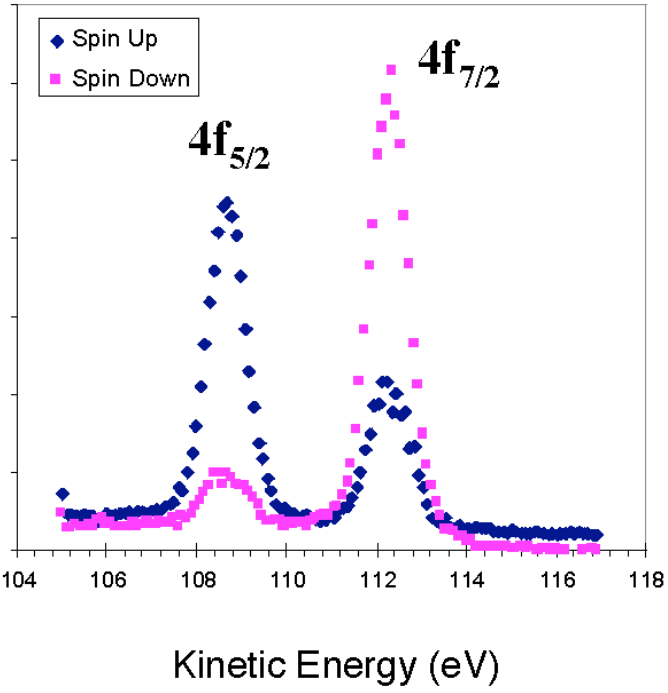

Figure 15. "Double Polarization" spectrum of Au(111) 4f peaks. Note that the combination of circularly polarized excitation with spin polarized detection can be used to produce spin polarized data from non-magnetic sample. The photon energy was 200 eV.

Last year, we reported are our preliminary low energy results for Double Polarization Photoelectron Spectroscopy of polycrystalline γ–Ce, using both circularly polarized x-rays and spin resolving detection. There were strong spin specific features (near 120- 122 eV KE) which reverse in spin polarity when the circular polarization helicity was reversed. (See Figure 16.) These measurements, near the 4d to 4f resonance, had been taken at the Advanced Light Source at LBNL in Berkeley, CA.

Now, we have expanded our Ce measurements to higher energy, using circularly polarized x-rays and true spin detection at the Advanced Photon Source at Argonne National Laboratory in Chicago, IL. (See Figure 17) These measurements were taken at the 3d to 4f resonance and confirm the lower energy measurements from the ALS.

Using circularly polarized x-rays and true spin detection via a MiniMott Detector, evidence of strong spin specific effects have been observed in the valence bands of ultrathin films of nonmagnetic Ce. (Fig 16 and 17) In the cases of the $3d^{5/2}$ to 4f and 4d to 4f transitions, there is a large static spin polarization across the entire valence band due to singlet coupling in the decay process, a type of electron correlation in the coulombically driven de-excitation route. For the 4d to 4f transition, a smaller oscillation in the vicinity of the lower Hubbard Band, near binding energies of 1 – 3 eV, is also observed. This smaller oscillation may be that for which we are looking, a manifestion of electron-electron correlation in the INITIAL STATES. However, the analysis here is complicated by the fact that the measurements were made on resonance in order to improve the counting rates. These "on resonance" measurements need to be repeated and extended to other photon energies.

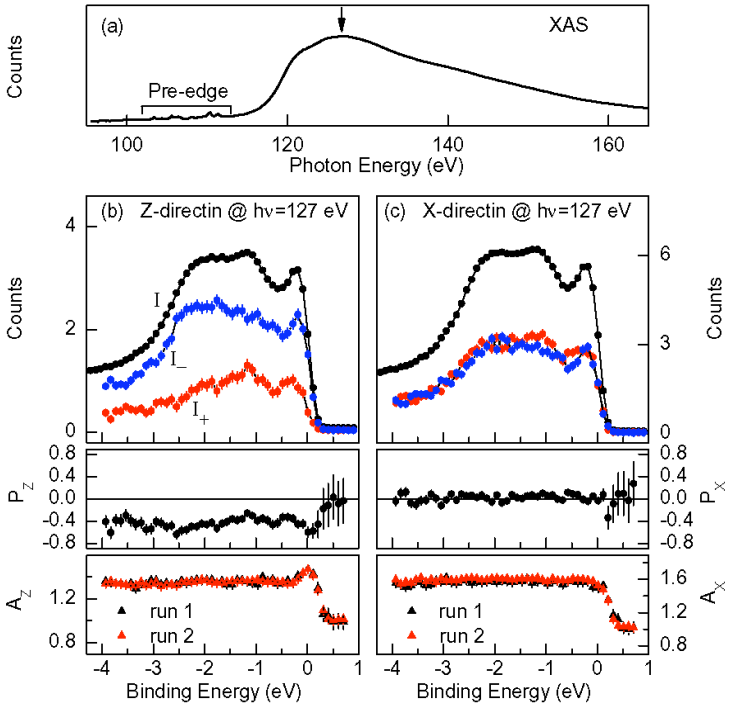

Figure 16 above

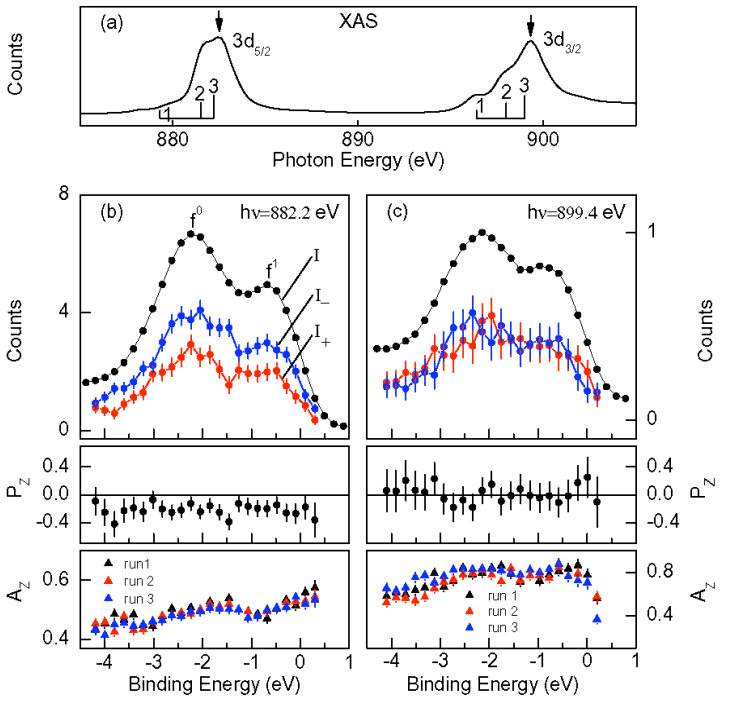

Figure 17 above

Figure 16
(a) XAS spectrum of Ce, showing the location of the RESPES expt.
(b) The spin resolved RESPES experiment, along the z-direction, with the spin polarized spectra in the top panel, the polarization (Pz) in the middle panel and the Instrumental Asym in the lowest panel. The measured spins and the photon helicity are along the z-direction.
(c) same as (b), but here the spins are along the x -direction, perpendicular to the helicity along the z – direction. Zero spin effect is expected in this configuration and none is observed.
Figure 17
RESPES results for the $3d_{5/2}$ and $3d_{3/2}$ resonances, with analogous definitions with Fig 16. Because a different spectrometer was used for these measurements, a slightly different experiment configuration was used here. Please see Yu et al, PRB 2006, for the experimental details.
A strong effect is observed at the $3d_{5/2}$ resonance but not at the $3d_{3/2}$ resonance. The absence of the effect at the $3d_{3/2}$ resonance is caused by the availability of an alternate Coster-Kronig decay path.

MCSNA:
Experimental Benchmarking of Pu Electronic Structure

The real issue here is the possibility of isolating spin-specific information about the Lower Hubbard (near 2 eV) and Kondo Peaks (at E_F). We seek to explore the nature of the Ce valence electronic structure, including the possibility of Kondo shielding in the peak at the Fermi energy. In order to do this, better resolution and off-resonance measurements are required. For this reason, lower energy experiments are now being performed, using a variant of the Linear Magnetic Dichroism technique, where a chiral configuration of vectors is constructed, using an un-polarized He source and spin detection. Preliminary results are shown in Figure 18.

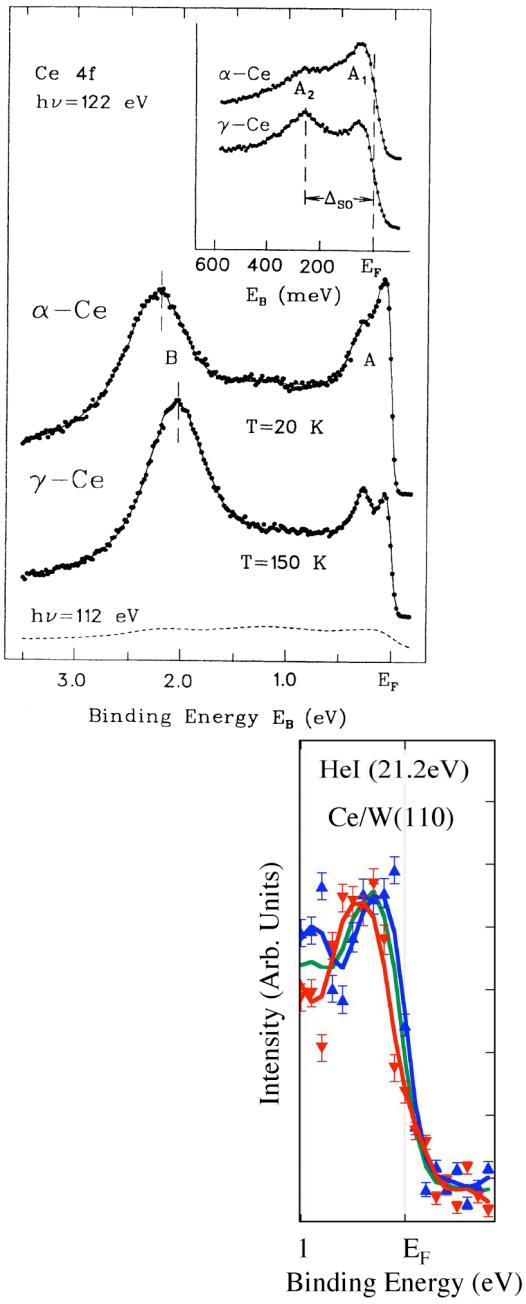

Figure 18

Top Panel- The high resolution, non-spin resolved results of Weschke et al., Reference 10. In their interpretation, they assign a spin-orbit splitting as the cause of the doublet near the Fermi Level.

Bottom Panel- Our preliminary spin resolved results for non-magnetic Ce/W, using He I as the excitation. Blue and red are spin resolved and green is spin-integrated.

Our spin resolved spectra confirm the interpretation of Weschke et al and demonstrate that we can indeed observe spin-orbit driven effects in the valence band structures of electron correlated Ce.

MCSNA:
Experimental Benchmarking of Pu Electronic Structure

IIIc In-house Fano Measurements of Pu Electronic Structure

We are confident that we have a good possibility to observe a Fano Effect in non-magnetic polycrystalline Pu, because we have already observed preliminary evidence of one in non-magnetic polycrystalline Ce. (See Figure 16 –18 above.) The spectra in Figure 16 -18 are essentially the fingerprint of a Kondo system. Thus, if Pu has no spin and orbital polarization but is "merely" Kondo shielded, we should observe this type of spectrum for Pu. If there is an underlying magnetic polarization in Pu, then we should observe something like that in Figure 12. One advantage that Pu has over Ce is that the counting rate should be 5 times higher: In Ce there is only one 4f electron: in Pu, there are five 5f electrons.

Plan to resolve the Pu 5f question

1. We will be performing the linear dichroic variant of the Fano Effect in-house, using a new hyper- intense He lamp and true spin detection. (Figure 19 below.)
2. We will start with polycrystalline Ce films and then move on to polycrystalline Pu.
3. By operating at the He II energy (40.8 eV), we will be sitting on a maximum in the Pu 5f cross section.
4. By working at LLNL, we can tap into the Pu sample handing and safety expertise of CMS/LLNL, i.e., Mark Wall.

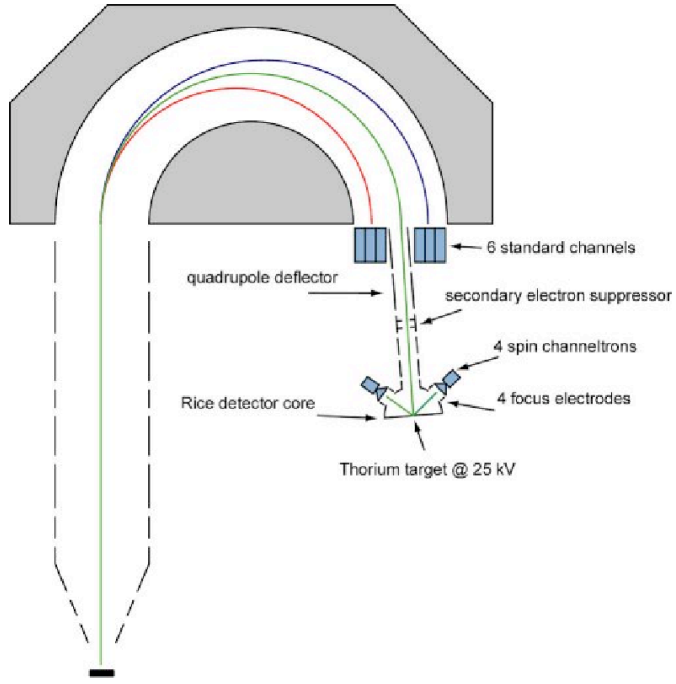

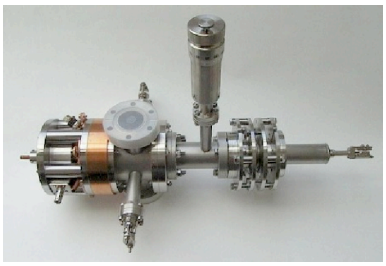

Figure 19 Instrumentation for the in-house Pu Fano Measurements.

We are proceeding with the construction of a dedicated, spin-resolving spectrometer for the study of Pu, with sophisticated safety features. We will use this Spectrometer to do the DPPS studies of Pu.

Top panel- New SPECS spin resolving analyzer in our lab.

Bottom panel- New SPECS hyper intense He source

MCSNA:
Experimental Benchmarking of Pu Electronic Structure

Ackowledgements

JGT gratefully acknowledges the support, aid and contributions of the following individuals. LLNL Collaborators: B.W. Chung, K.T. Moore, S.- W. Yu, A.J. Schwartz, M.A. Wall, S.A. Morton, B.B. Ebbinghaus, M.J. Fluss, J.J. Haslam, K.J.M. Blobaum, J.Terry, R.K. Schulze, J. Lashley, J.D. Farr, T. Zocco, M. Blau, K. Heizelmann, E. Rotenberg, D.K. Shuh, G. van der Laan, A.L. Kutepov, T. Komesu, and G.D. Waddill. This work was performed under the auspices of the U.S. DOE by University of California Lawrence Livermore National Laboratory under contract W-7405-Eng-48. Work by LLNL personnel was funded in part by the Office of Basic Energy Science at DOE. The APS, ALS and the Beamline 4 Spectromicroscopy Facility have been built and operated under funding from the Office of Basic Energy Science at DOE.

References

1. Y. Baer and G. Busch, Phys. Rev. Lett. 31, 35 (1973).
2. D. Wieliczka, J.H. Weaver, D.W. Lynch, and C.G. Olson, Phys. Rev. B 26, 7056 (1982).
3. E. Wuilloud, H.R. Moser, W.D. Schneider, and Y. Baer, Phys. Rev. B 28, 7354 (1983).
4. D.M. Weiliczka, C.G. Olson, and D.W. Lynch, Phys. Rev. B 29, 3028 (1984).
5. D.M. Weiliczka, C.G. Olson, and D.W. Lynch, Phys. Rev. Lett. 52, 2180 (1984).
6. E. Jensen and D.M. Weiliczka, Phys. Rev. B 30, 7340 (1984).
7. F. Patthey, B. Delley, W.D. Schneider, and Y. Baer, Phys. Rev. Lett. 55, 1518 (1985).
8. C. Laubschat, E. Weschke, C. Holtz, M. Domke, O. Strebel, and G. Kaindl, Phys. Rev. Lett. 65, 1639 (1990).
9. F. Patthey, J.M. Imer, W.D. Schneider, H. Beck, Y. Baer, and B. Delley, Phys. Rev. B 42, 8864 (1990).
10. E.Weschke, C. Laubschat, T. Simmons, M. Domke, O. Strebel, and G. Kaindl, Phys. Rev. B 44, 8304 (1991).
11. Y. Baer, M. Grioni, D. Malterre, and W.D. Schneider, Phys. Rev. B 44, 9108 (1991).
12. J.J. Joyce, A.J. Arko, J. Lawrence, P.C. Canfield, Z. Fisk, R.J. Bartlett, and J.D. Thompson, Phys. Rev. Lett. 68, 236 (1992).
13. L.Z. Liu, J.W. Allen, O. Gunnarsson, N.E. Christensen, and O.K. Anderson, Phys. Rev. B. 45, 8934 (1992).
14. E. Weschke, A. Hoehr, G. Kaindl, S. L. Molodstov, S. Danzenbaecher, M. Richter and C. Laubschat, Phys. Rev. B 58, 3682 (1998).
15. O. Gunnarsson and K. Schoenhammer, Phys. Rev. Lett 50, 604 (1983).
16. O. Gunnarsson and K. Schoenhammer, Phys. Rev. B 28, 4315 (1983).
17. J.W. Allen and J.Z. Liu, Phys. Rev. B 46, 5047 1992).
18. B. Johansson, I.A. Abrikosov, M. Alden, A.V. Ruben, and H.L. Skriver, Phys. Rev. Lett. 74, 2335 (1995).
19. K. Held, A.K. McMahan, and R.T. Scarlettar, Phys. Rev. Lett. 87, 276404 (2001).
20. E. Weschke, C. Laubschat, R. Ecker,A. Hoehr, M. Domke, G. Kaindl, L. Severin and B. Johansson, , Phys. Rev. Lett. 69, 1792 (1992).
21. D. Malterre, M. Grioni, Y. Baer, L. Braichovich, L. Duo, P. Vavassori, and G.L. Olcese, Phys. Rev. Lett. 73, 2005 (1994).
22. E. Weschke, C. Laubschat,A. Hoehr, M. Domke, G. Kaindl, L. Severin and B. Johansson, , Phys. Rev. Lett. 73, 2006 (1994).
23. A.J. Arko, J.J. Joyce, A.B. Andrews, J.D. Thompson, J.L. Smith, D. Mandrus, M.F. Hundley, A.L. Cornelius, E. Moshopoulou, Z. Fisk, P.C. Canfield, and A. Menovsky, Phys. Rev. B 56, R7041 (1992).
24. G. Kotliar and D. Vollhardt, Physics Today **57,** 53 (March 2004).
25. U. Fano, Phys. Rev. **178**, 131 (1969); **184**, 250 (1969).
26. M.S. Lubell and W. Raith, Phys. Rev. Lett. 23, 211 (1969).
27. J. Kessler and J. Lorenz, Phys. Rev. Lett. 24, 87 (1970).
28. G. Baum, M.S. Lubell, and W. Raith, Phys. Rev. Lett. 25, 267 (1970).
29. U. Heinzmann, J. Kessler, and J. Lorenz, Phys. Rev. Lett. 25, 1325 (1970).
30. U. Heinzmann, H. Heuer, and J. Kessler, Phys. Rev. Lett. 34, 441 (1975); 34, 710 (1975).
31. Schoenhense, U. Heinzmann, J. Kessler, and N.A. Cherepkov, Phys. Rev. Lett. 48, 603 (1982).
32. B.Vogt, B. Kesser, N. Mueller, G. Schoenhense, B. Schmiedeskamp, U. Heinzmann, Phys. Rev. Lett. 67, 1318 (1991).
33. K. Starke, A. P. Kaduwela, Y. Liu, P. D. Johnson, M. A. Van Hove, C. S. Fadley, V. Chakarian, E. E. Chaban, G. Meigs, and C. T. Chen, Phys. Rev. B 53, R10544 (1996).
34. C. Roth, F.U. Hillebrecht, W.G. Park, H.B. Rose, and E. Kisker, Phys. Rev. Lett. 73, 1963 (1994).
35. H.B. Rose, A. Fanelsa, T. Kinoshita, C. Roth, F.U. Hillebrecht, and E. Kisker, Phys. Rev. B. 53, 1630 (1996).